AL22 - Alucell Latest Development: Modelling Impact of CO_2 Bubbles and Anode Slot Configuration on Liquid Flows in Hall-Héroult Pot

Nadia Chailly[1], André Augé[2], Alexandre Masserey[3], Julien Hess[4], Jacques Rappaz[5] and Emile Soutter[6]
1. Modeling Engineer, PhD.
2. Senior Data Scientist
Rio Tinto Aluminium Pechiney - LRF, Saint-Jean-de-Maurienne, France
3. Physical Engineer, PhD.
4. Mathematical Engineer
Ycoor Systems SA, Sierre, Switzerland
5. Professor, Scientific Consultant
EPFL - Institute of Mathematics, Lausanne, Switzerland
6. Computational Engineer, PhD.
Corintis SA, Lausanne, Switzerland
Corresponding author: nadia.chailly@riotinto.com

Abstract

During the aluminum electrolysis process, CO_2 bubbles are generated under the anodes and released through anode slots. To study the impact of these bubbles on bath flows and therefore to help understand related phenomena observed in an aluminum reduction pot, a mixture model of CO_2 bubbles diluted in a liquid bath was developed and integrated into Alucell software. Alucell is a suite of numerical simulation models which calculates magnetohydrodynamics (MHD), alumina dissolution as well as the coupling between thermo-electric balance and MHD flow.

This article explains how equations are modified in Alucell in relation with the latest mixture model developed. The effect of the gas on bath velocity, and metal pad upheaval is demonstrated. Furthermore, the impact of anode slot configurations on bubbles and liquid flow behavior is also investigated. Modeling results were analyzed and compared to some observed phenomena in the aluminum reduction pots.

Keywords: Alucell, mixture model, liquid flows, bubbles, slotted anodes

1. Introduction

Industrial aluminum production is based on the Hall-Héroult electrolysis process. The electrochemical reduction occurs in molten electrolyte (bath) maintained at 970 °C in a pot where high quantities of electrical energy are needed. The latest generation of pots is very large with current greater than 600 kA. Direct electric current passes continuously from the anode to the cathode allowing electrolysis of alumina (Al_2O_3) with carbon anodes to produce molten aluminum, as shown in Equation (1)

$$2Al_2O_3 + 3C = 4Al + 3CO_2 \quad (1)$$

Since carbon anodes takes part in the chemical reaction, carbon dioxide (CO_2) is generated under the anodes by the reaction of carbon with oxygen leading to the consumption of anodes, which have to be replaced regularly. CO_2 bubbles influence electrical and hydrodynamic behavior of the pot in both positive and negative ways. Gas bubbles induce bath flow and play a significant role in the alumina mass transfer, resulting in better alumina dissolution and alumina transport in the bath. On the other hand, since most of the bath is covered by the anodes, a nearly continuous layer of gas could be generated underneath the anodes through bubble collision and coalescence. Such

a gas layer can cover a large part of the anode surface up to 90 percent of its surface, according to modelling [1]; this increases electrical resistance between the anode and the bath and can significantly raise the pot voltage and eventually decreases the performance of the pot.

Several ways are used by the aluminum industry to optimize its production and reduce energy consumption. In recent years, some solutions were based on the optimization of electrical and geometrical configurations of the pot. Among others, slotted anodes have been used by aluminum smelters to reduce gas coverage and gas bubble layer resistance [2, 3]. Indeed, the slots encourage a quick evacuation of the bubbles from the bottom of the anodes, and slot effectiveness depends on their dimensions, positions, and orientation. For a good control of the electrolysis process, understanding the movement as well as the behavior of the gas bubbles is essential. Due to the complexity of the flow field measurements in the extreme pot operating conditions, numerical simulation is often used to understand and describe the complex flows inside the pot. Such flows involve multiphase coupling between liquid, bubbles, and alumina dissolution.

In the past years, some studies have been carried out where only gas driven flow has been considered [4, 5]. Other studies were done without considering the impact of magnetohydrodynamic effects and/or metal-bath interface fluctuations. We can quote the work of Wang et al. [6] who developed a multiphase flow model to study the gas driven flow without considering the effect of magnetic forces. Their model was validated with measurements in a full-scale water model. Yang et al. [7] also ignored the influence of the magnetic forces in their numerical simulation modeling. Wang et al. [8] studied the behavior of the gas bubbles in a water model to define the optimum slotted anode design without considering bath metal interface movement. Recently, Meijia et al. [9] developed a two-phase model coupled with magnetohydrodynamic aspects to investigate the effect of slotted anodes on the gas bubble movement with the consideration of the bubble coalescence. The model was developed on a pair of anodes only.

Indirectly, the impact of the bubble release from the slots during the anode cycle is observed experimentally on the increase of the sidewall temperatures and a local decrease of ledge thickness.

To consider these complex coupling phenomena, in this work we focused on the modeling of the gas-bath mixture flow at the level of the whole aluminum reduction pot. This paper presents the Alucell's latest development where the equations of the steady state model are modified to include the presence and the movement of the CO_2 bubbles.

2. Model Description

The global effect of the CO_2 bubbles on the bath flow is studied without considering bubble nucleation and coalescence. Since the typical size of the whole pot is several meters whereas the size of a gas bubble is a few millimeters, we adopted a statistical averaged model, namely a dilute dispersion of gas bubbles in liquid bath, described by Soutter [10]. Our model is coupled with magnetohydrodynamics and free surface calculations, and is incorporated in Alucell for industrial simulations.

Alucell is a unique suite of numerical simulation models which has been developed over thirty years in partnership between Rio Tinto, Ecole Polytechnique Fédérale de Lausanne (EPFL) and Ycoor Systems. The software comprises five different physics-based models as described by Renaudier et al. [11]. In these coupled models, magnetohydrodynamic stability (MHD) of the pots, alumina dissolution and thermal balance with ledge calculation are performed.

The steady state model is the core of the suite and it represents the starting point for the other models. It calculates the electrical current distribution, the magnetic field including ferromagnetic effects due to the presence of steel, the liquid metal and bath velocity field and the metal pad upheaval. All the details of the stationary calculations, including the aluminum-bath interface are described by Flueck et al. [12, 13] and Steiner [14].

2.1 Mixture Model for Diluted CO_2 Bubbles in the Liquid Bath

The mixture model of two-phase flow consisting of gaseous phase diluted into a liquid phase is presented in this sub-section. All the details of the model are described by Soutter [10]. The general Navier-Stokes equations with varying density are used. The equations of conservation of mass and momentum for each phase are combined, and the resulting equations are Navier-Stokes equations with varying density. The model is expressed in Eulerian form; thus, the gas bubbles are not represented. Both bath and gas are considered as incompressible fluids with constant density and with the same pressure (by neglecting the capillary pressure and surface tension forces as well).

The conservation of the volume implies (2):

$$\alpha_g + \alpha_b = 1 \tag{2}$$

Based on the principle of mass and momentum conservation for the mixture, the density of the bath-gas mixture ρ_m and its velocity u_m are defined in Equation (3), and Equation (4):

$$\rho_m = \rho_g \alpha_g + (1 - \alpha_g)\rho_b \tag{3}$$

$$\rho_m u_m = \alpha_g \rho_g u_g + (1 - \alpha_g)\rho_b u_\mathrm{b} \tag{4}$$

Thus, by neglecting the capillary pressure of the gas and the Reynolds stress tensor [10], the motion of the bath-gas mixture can be described by the Equation (5), and Equation (6), which are the Navier-Stokes equations for the mixture:

$$\frac{\partial}{\partial t}(\rho_m u_m) + div(\rho_m u_m \otimes u_m) - div(\tau_m) = j \otimes B + \rho_m \mathrm{g} \tag{5}$$

$$\frac{\partial \rho_m}{\partial t} + \mathrm{div}(\rho_m u_m) = 0 \tag{6}$$

With τ_m, the stress tensor of the mixture defined in the Equation (7), and $\epsilon(u_m)$ the mixture strain rate tensor given by the Equation (8):

$$\tau_m = 2\mu_m \epsilon(u_m) - \frac{2}{3}\mu_m div(u_m)\mathbf{I} - p \tag{7}$$

$$\epsilon(u_m) = \frac{1}{2}(\nabla u_m + (\nabla u_m)^T) \tag{8}$$

The momentum conservation of the gas is described by the Equation (9):

$$\frac{\partial}{\partial t}(\alpha_g \rho_g u_g) + div(\alpha_g \rho_g u_g \otimes u_g) - div(\tau_g) = \alpha_g \rho_g \mathrm{g} - \alpha_g \nabla \mathrm{p} + F_D \tag{9}$$

With τ_g, the stress tensor of the gas described by the Equation (10), and $\epsilon(u_g)$ the gas strain rate tensor given by the Equation (11):

$$\tau_{\mathrm{g}} = -p\alpha_g \mathbf{I} + \mu_g \left(-\frac{2}{3} div(u_g)\mathbf{I} + 2\epsilon(u_g)\right) \quad (10)$$

$$\epsilon(u_g) = \frac{1}{2}\left(\nabla u_g + (\nabla u_g)^T\right) \quad (11)$$

F_D is the drag force corresponding to the Stokes's law, described by the Equation (12), where D is the drag force coefficient given by the Equation (13):

$$F_D = D\alpha_g(1 - \alpha_g)(u_b - u_g) \quad (12)$$

$$D = \frac{18\mu_g}{d^2} \quad (13)$$

As described by Steiner [13], the turbulence model is a mixing length model composed of a laminar part and a turbulent part. The viscosity μ is defined in the Equation (14):

$$\mu_i = \mu_{i,L} + \mu_{i,T} = \mu_{i,L} + \rho C_T h^2 \sqrt{2\epsilon(u_i) : \epsilon(u_i)} \quad (14)$$

Where L denotes the laminar part, T denotes the turbulent part with $i \in \{m(mixture), g(gas)\}$.

Finally, the mass conservation of the gas leads to the Equation (15):

$$\frac{\partial \alpha_g}{\partial t} + div(\alpha_g u_g) - div(\mathrm{K}\nabla\alpha_g) = \dot{\alpha}_g \quad (15)$$

With $\dot{\alpha}_g$, the gas production source per unit time due to the chemical reaction described in the Equation (1). The gas diffusion coefficient K is also composed of linear part and turbulent part by similarity to the viscosity approximation [10].

In these equations:

ρ_m	Density of the mixture, kg/m^3
ρ_g	Density of the gas, kg/m^3
ρ_b	Density of the bath, kg/m^3
α_g	Gas volume ratio
α_b	Bath volume ratio
g	Acceleration of gravity, m/s^2
u_m	Mixture velocity vector of the fluid, m/s
τ_{m}	Mixture stress tensor, kg/m^{2}s^2
ϵ	Strain rate tensor,1/s
μ_m	Local viscosity of the mixture, Pas
j	Electric current density vector, A/m^2
B	Magnetic induction vector, T
$\otimes$	Vector cross product
p	Pressure, Pa
$\mathbf{I}$	Identity matrix
T	Denotes vector transpose
u_g	Velocity vector of the gas, m/s
u_b	Velocity vector of the bath, m/s
τ_{g}	Gas stress tensor, kg/m^{2}s^2
μ_g	Gas viscosity, Pas
F_D	Drag force, kgm/s^2
D	Drag coefficient, kg/m^{3}s

d Average diameter of gas bubbles, m
$\dot{\alpha}_g$ Gas source term, l/s
K Gas diffusion coefficient, m^2/s
C_T Turbulence parameter, m^2
h Typical mesh element size, m

The stationary mixture velocity u_m and the pressure p are numerically computed using a finite element method by solving the Equations (5) and (6). The velocity of the gas u_g and the gas distribution α_g are computed from Equations (9) and (15).

2.2 Results

In this work an AP-30 technology pot of Rio Tinto is studied. The geometry of the model is presented in the Figure 1. As it is shown, the whole pot is modeled. To investigate the impact of the slotted anodes on the bubble release, and considering the complexity of the structures, only two anodes situated in the middle of the pot (downstream side) have two longitudinal slots each, inclined towards the lateral side. Two configurations of the slots are studied. The first one corresponds to the case where the slots are not yet fully immersed into the bath, whereas the second one corresponds to the case where the slots are immersed into the bath.

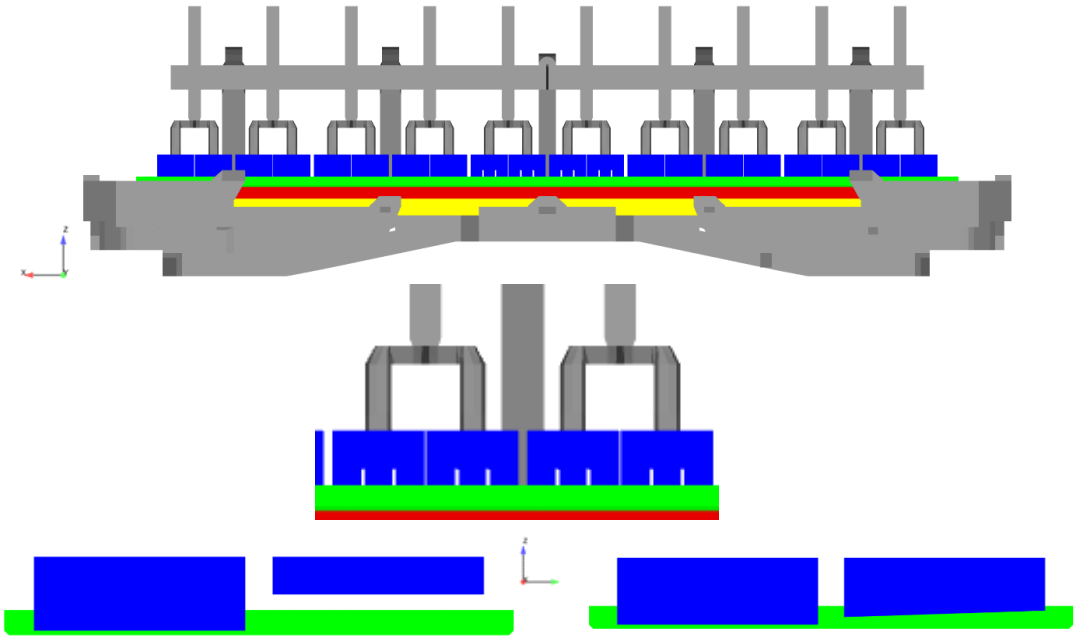

Figure 1. Geometry model. Top: pot with two slotted anodes in the center. Left: non-immersed slots. Right: immersed slots.

In order to obtain a reference solution, the simulations were first performed without slotted anodes and without CO_2 gas bubbles. Then, based on the same specifications as the reference case, the calculations were done with the gas, considering a bubble diameter of 4 mm but without slots. Finally, the case with gas was performed using the slotted anodes with the two configurations mentioned above.

The gas bubbles are produced into the bath from anode bottoms (proportional to the current density) and escape from the bath top surface. The total CO_2 gas production in the bath, ($\dot{\alpha}_g$) is about 0.035 kg/s for a pot operating at 320 kA and 95 % current efficiency (CE).

For the reference case, corresponding to MHD driven flow only, the streamlines in the bath flow are plotted in Figue 2. We can see that the main eddies are located on both ends of the pot, atwond that there is a small eddy at each downstream corner. The velocity is maximum at the upstream corners and smaller on the downstream corners with the reverse eddies. The maximum velocity in the bath is about 13 cm/s.

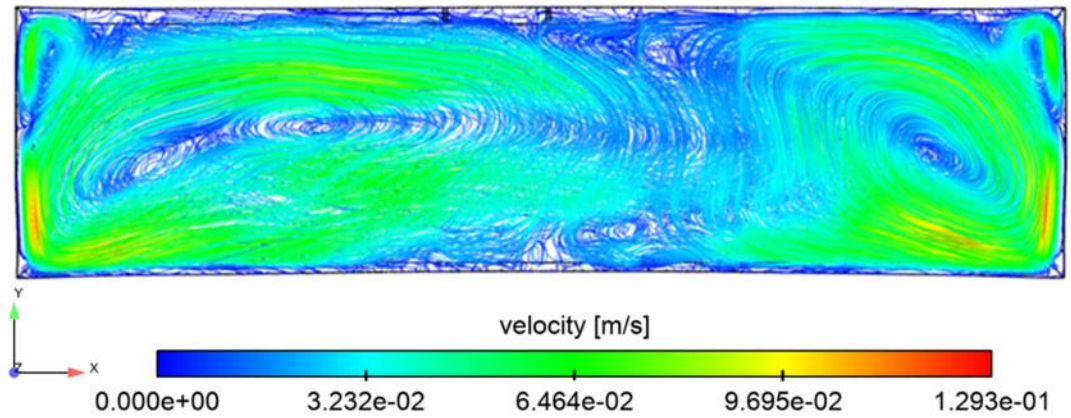

Figure 2. Bath velocity field in the bath for the reference case.

When the gas is considered in the model, the mixture velocity u_m is solved in the whole liquid domain (aluminum and bath) while the gas velocity u_g and gas fraction α_g are solved in the bath only. Figure 3 shows the map of the difference between the mixture velocity obtained by the model with gas and the one obtained without gas, at the middle of anode-cathode distance (ACD).

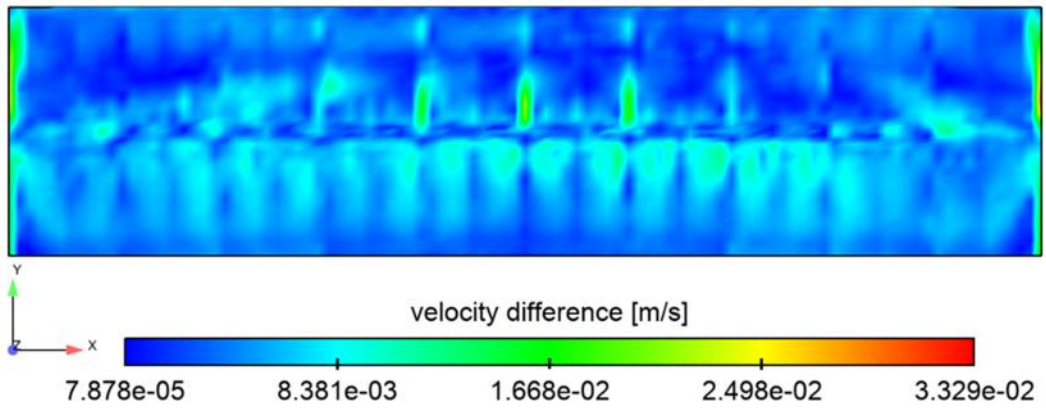

Figure 3. Bath (mixture) velocity difference between the case with gas and the reference case at the middle of ACD.

The effect of the gas on the liquid flow is measured at maximum 30 % of change. The most noticeable change of the velocity is observed under the channels (lateral and central) with velocity difference of up to 3.5 cm/s. The gas velocity can be seen in Figure 4. On the top, the map of the velocity field is shown at the bath free surface. Gas velocity is noticeable at the central and lateral channels where the gas can escape easily. On the bottom, velocity vectors show the gas release with gas velocity amplitude reaching up to 20 cm/s.

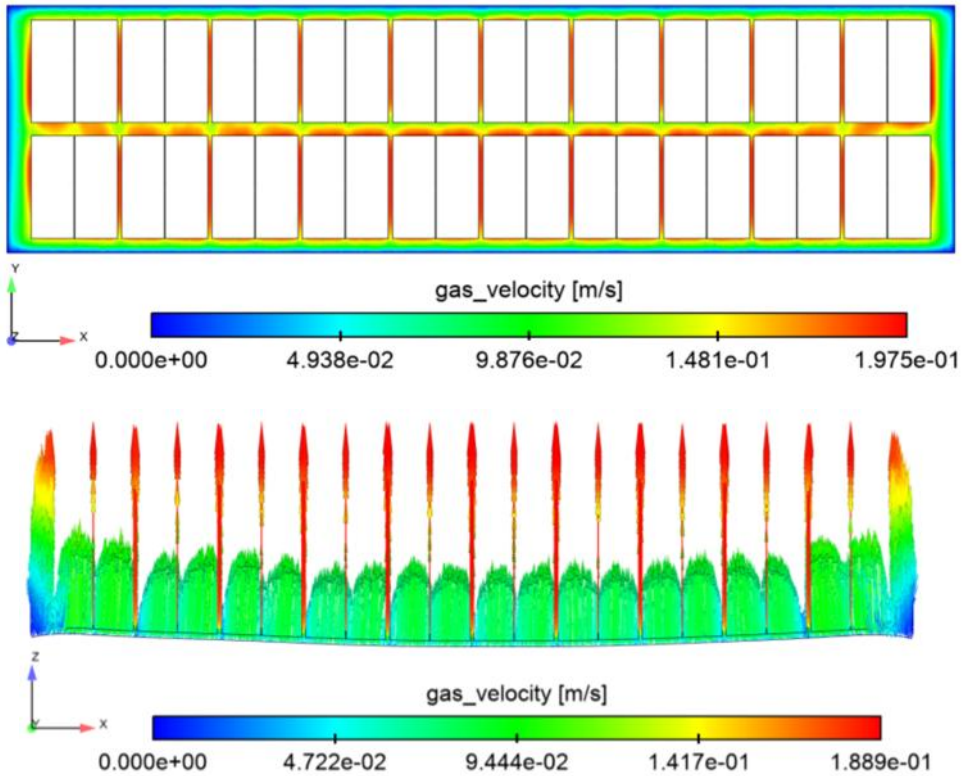

Figure 4. Gas velocity for the case without slots. Top: at the bath free surface. Bottom: in a vertical cutting plane.

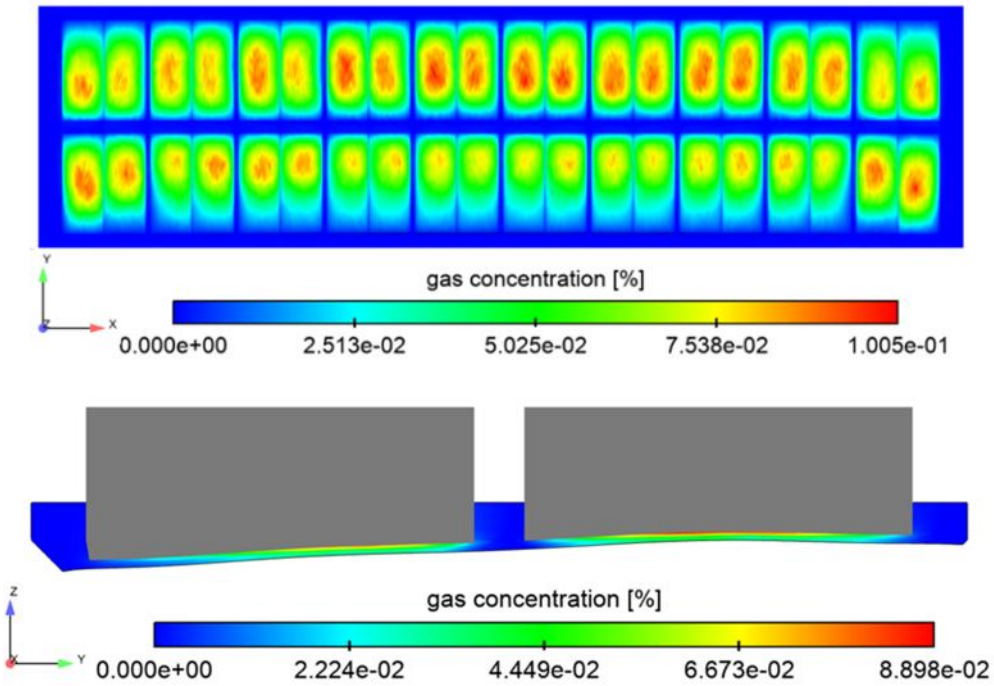

Figure 5. Gas distribution α_g for the case without slots. Top: middle of ACD. Bottom: cut view.

Figure 5 illustrates the gas concentration α_g, in the case without slots, at the middle of ACD on the top, and under two anodes in a cut view, on the bottom. The gas concentration is higher mostly under the anodes since the gas escapes up quickly once in the channels.

This gas distribution seems to be at the origin of the change on the metal pad interface as seen in Figure 6, which shows the metal height difference between the case with gas and without slots, and the reference case. It is noticed that the locations where a lot of gas is present, the alleviated mixture density leads the interface to lift upwards. In particularly, the red areas correspond to the move upwards of the interface (+ 1.6 cm) when the gas is included, corresponding approximately to areas where gas distribution α_g is concentrated under the anodes as shown in the Figure 5 above.

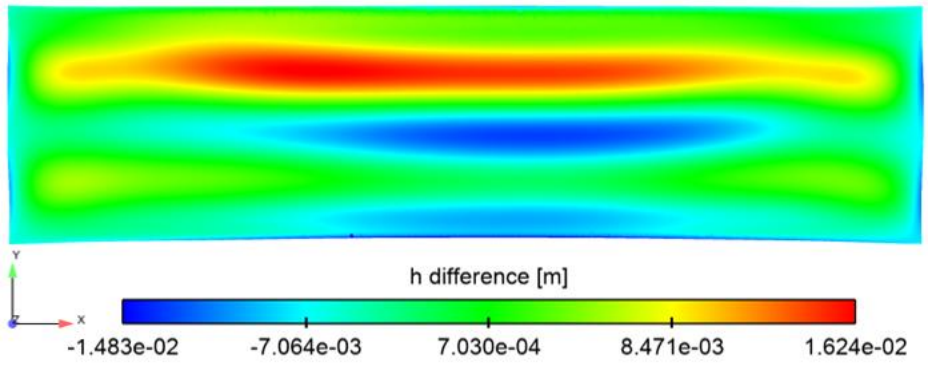

Figure 6. Metal height difference h – $h_{reference}$ (without gas).

The gas distribution α_g obtained in the case of non-immersed slots is presented in Figure 7. Thanks to the slots to evacuate the bubbles directly upwards to the bath free surface, we can see that under the slotted anodes, the gas concentration is approximately four times lower than under the other anodes.

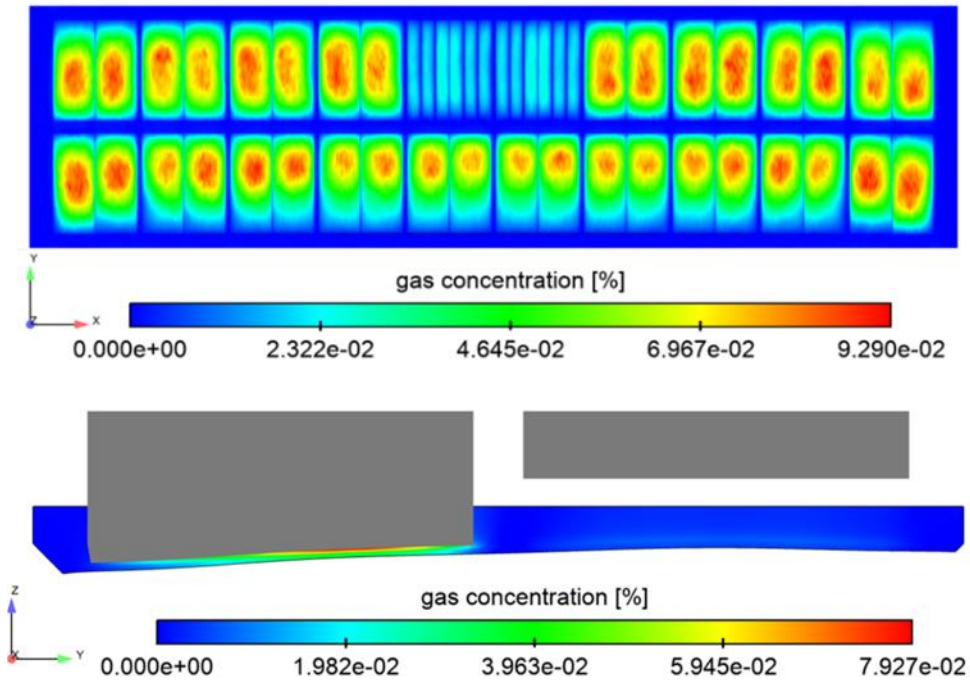

Figure 7. Gas distribution α_g for the case with two slotted anodes, slots not yet immersed. Top: middle of ACD. Bottom: cut view.

When the inclined slots are immersed into the bath, the gas is released towards the lateral channel. This can be observed in the Figure 8. A few remarks can be made in this case. The gas

concentration α_g under the anodes without slots is around 10 % and remains in the same order of magnitude of the values obtained in the case with gas and without slots (Figure 5). If we look under the slotted anodes, the quantity of gas is increased, with a particularly important accumulation at the lateral side of the pot, but inside the slot. The gas concentration reached there is approximately 36 %.

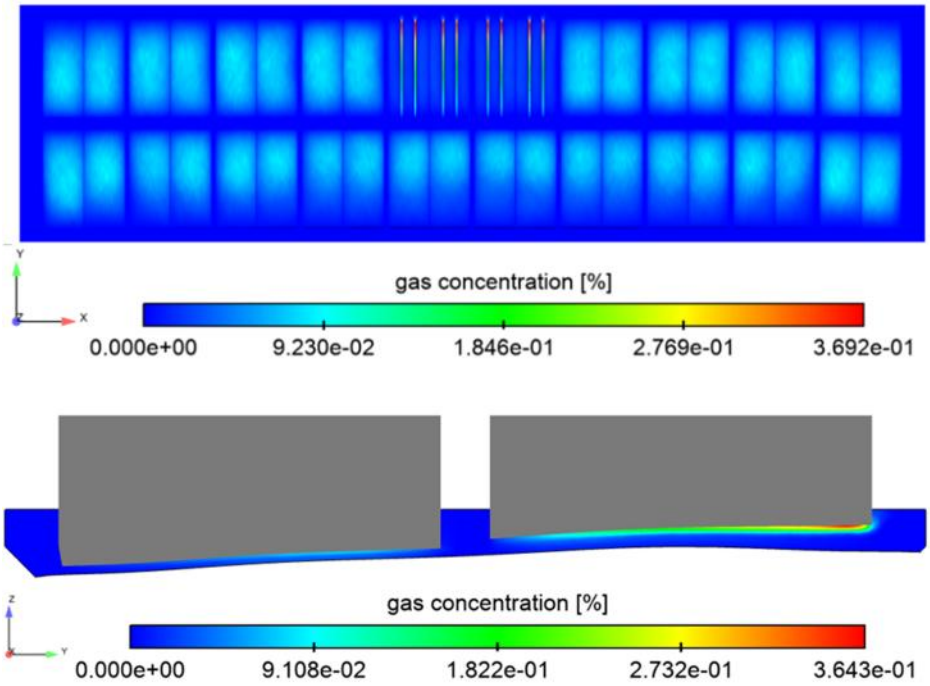

Figure 8. Gas distribution α_g for the case with two slotted anodes, slots immersed and inclined. Top: middle of ACD. Bottom: cut view.

Figure 9 shows that the upwards movement of the bubbles to the top of the bath free surface is generally observed in the 3 configurations: (1) with slots not immersed yet, (2) with inclined immersed slots, and (3) with consumed slots.

In the configuration (1), bubbles are evacuated mainly upwards the bath free surface, thus the variation of the gas velocity values between the configuration (1) and the configuration (3) seems negligeable (except inside the slot). The maximum of velocity magnitude for both cases is around 19 cm/s. In the configuration (2), when the slots are immersed, the gas is evacuated with higher velocities, with a maximum value of 22 cm/s.

Figure 10 shows the mixture velocity in the bath for the 3 configurations already mentioned above. Among these configurations, it is noticeable that the configuration (2), is the one which induces higher mixture velocities. We can see that the maximum velocity is increased significantly from 6 cm/s, in the configuration (1) to 14.2 cm/s, in the configuration (2). This is noticeable in the slots, at the extremity of the anode, near the lateral channel side. On one hand, the bubbles escaping from the slots generates an upwards flow and on the other hand, the bubbles push the bath with high velocities towards the sidewall, leading to strong recirculation zones in the lateral channel. In the configuration (3), when the slots are consumed, the bubbles are mainly evacuated and dispersed around the anode, thus the mixture velocities are lower with a maximum value of 3.8 cm/s

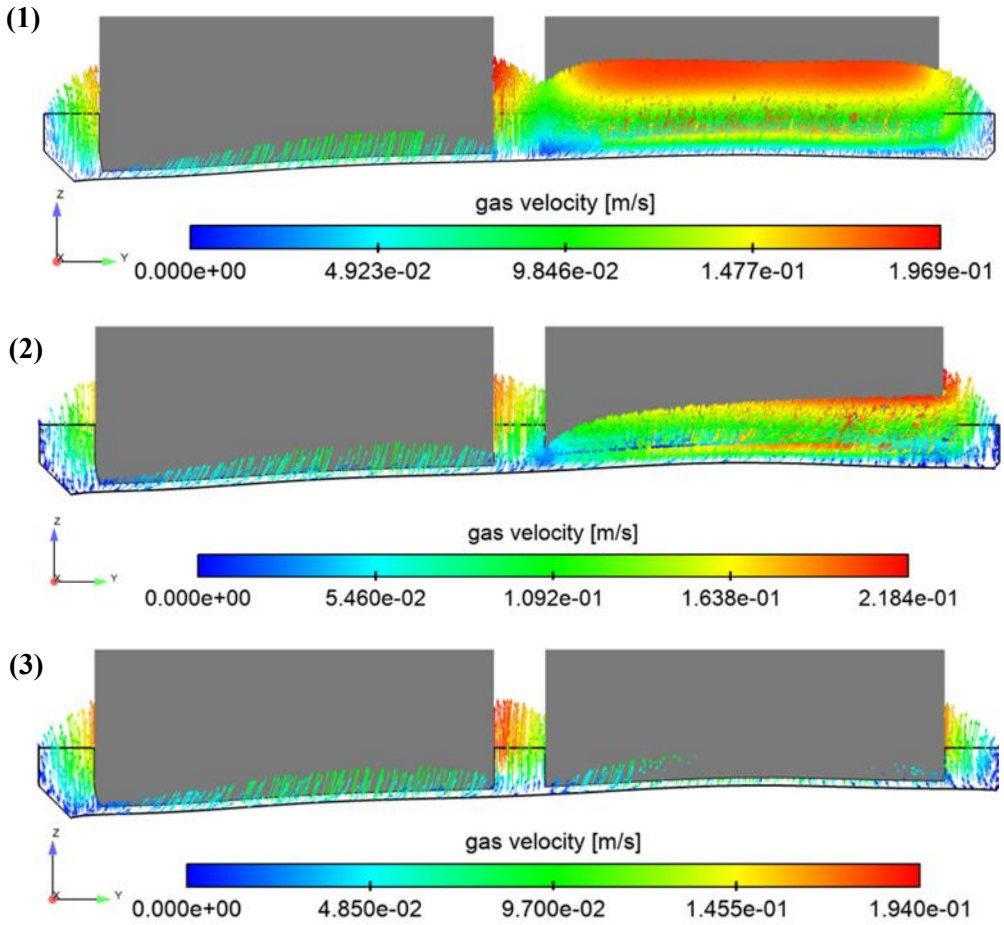

Figure 9. Gas velocity u_g. Top: non-immersed slots. Middle: immersed slots. Bottom: without slots.

3. Model Validation

Due to the difficulties to perform direct measurements of the flow field in aluminum reduction harsh operating conditions, the model is validated qualitatively using temperature measurements. Indeed, we exploited some measurements performed on a prototype pot installed in the Laboratoire de Recherche des Fabrications (LRF) of Rio Tinto, in Saint Jean de Maurienne. As the LRF pots are dedicated to R&D, they are equipped with numerous continuous measurements, unlike pots in industrial smelters. Thus, the impact of CO_2 bubbles released by the slots on the temperature of the pot shell was investigated and related to the numerical simulation results and observations.

3.1 Measurements Description

Several thermocouples are placed on the pot sidewall at different heights of the cathode as shown in the left side of the Figure 11. These thermocouples are connected to the Alpsys® system and therefore continuous monitoring of temperatures during the anode cycle is enabled. The temperature measurements are distributed along the upstream and the downstream side as shown in the right side of the Figure 11. Four levels of measurements are aligned vertically from the bottom to the top. In this work, we focused on the measurements of the thermocouples situated at the *bath free surface (*level 4). The used anodes have two longitudinal slots inclined towards the lateral side.

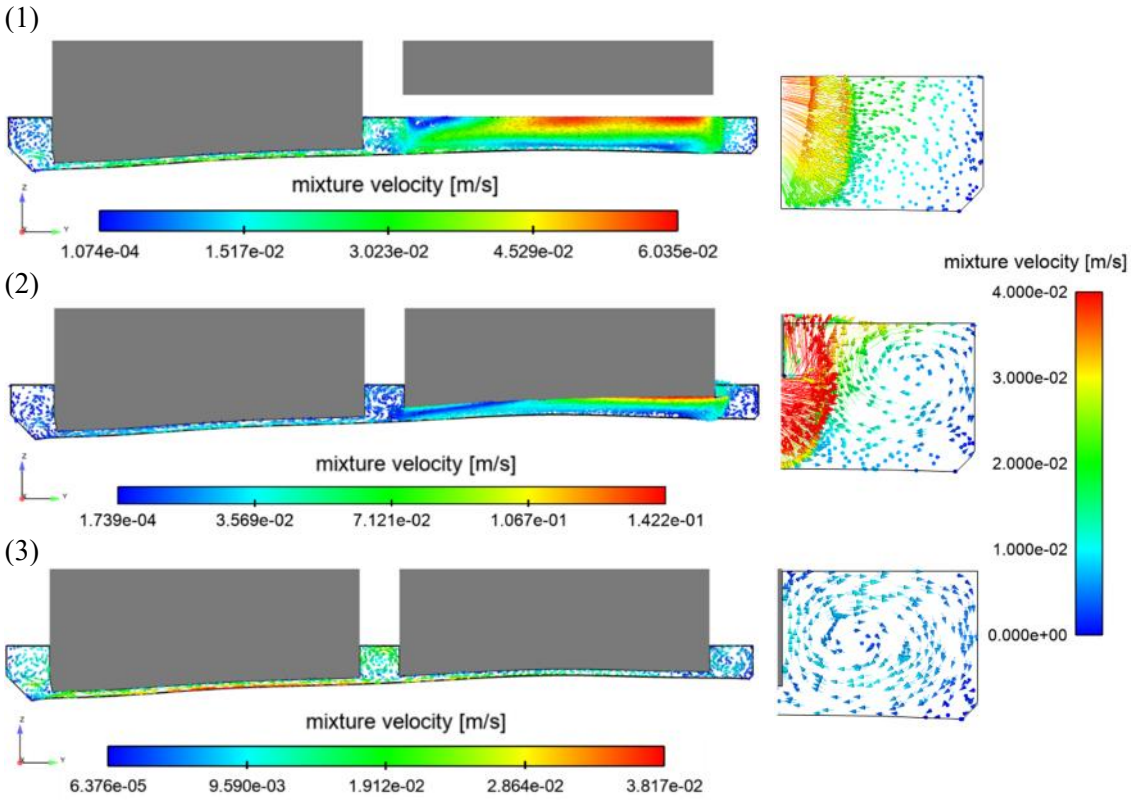

Figure 10. Mixture velocity u_m. Top: non-immersed slots. Middle: immersed slots. Bottom: without slots.

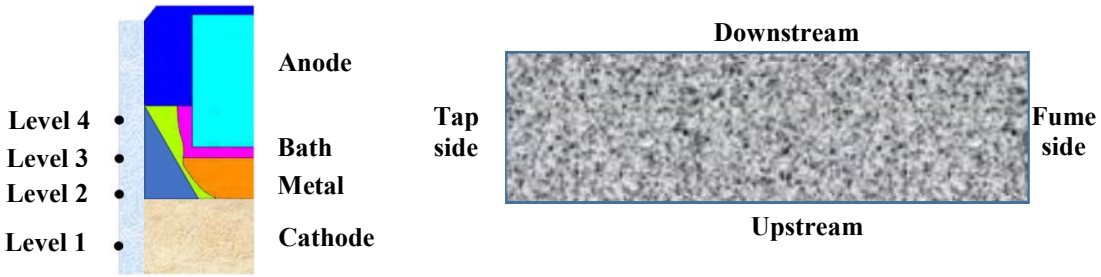

Figure 11. Left: thermocouples' positions at the pot side wall. Right: pot top view.

During the anode cycle, three main phases are observed as schematized in the Figure 12. At the beginning, the anode is cold and causes the bath solidification and the cooling of the pot sidewall as well. The slots are not completely immersed into the bath hence the CO_2 bubbles can escape through the slots to the bath free surface. In this case, bath stirring is very low or possibly non-existent.

After 240 hours, the slots are immersed into the bath up to 460 hours approximatively. The bubbles collected in the slots are released in the bath towards the lateral channels. Therefore, on one hand high bath stirring is induced, and on the other hand, the hot bath is pushed by the gas bubbles towards the lateral sidewall of the pot. This phenomenon may be the origin of gradual melting of the ledge profile and wall temperatures increase.

Finally, when the slots disappear, after 460 hours, the bubbles are dispersed around the anode and the mixing of the bath in the lateral channel is lower.

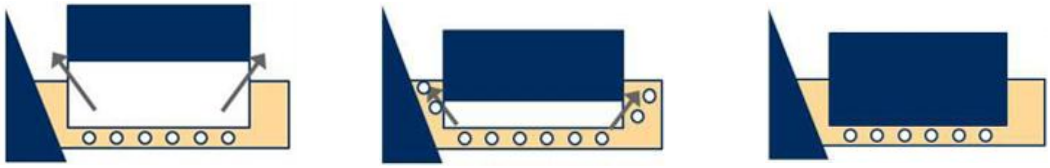

Figure 12. Schematization of anode slots cycle in the aluminum reduction pot. Left: no immersed slot. Middle: immersed slot. Right: consumed slot.

3.2 Statistical Analysis of the Measurements

The statistical analysis was carried out by André Augé, Senior Data Scientist from the LRF team, using the worldwide statistical software JMP®. The study is based on the measurements performed over 11 anode cycles, knowing that the initial moment (t=0) for the follow-up corresponds to the moment when the anode is set up in the pot. The temperature measurements as a function of the age of the anode can be observed on the Figure 13, for *bath free surface*, at upstream (on the left) and downstream (on the right).

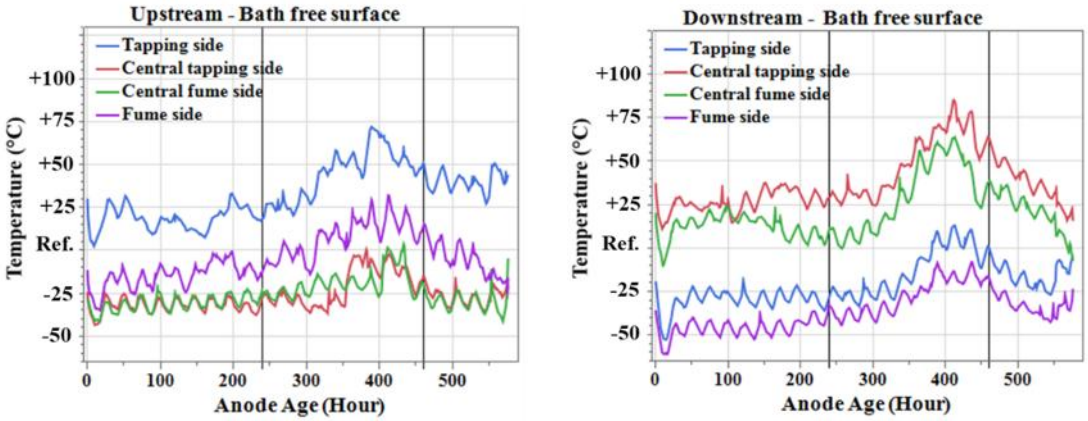

Figure 13. Temperature variations at bath free surface.

We can see that all the measurements have daily fluctuations of a few degrees (10 °C max) due to variations in daytime and nighttime temperatures. Small wavelets can be observed at the upstream as well as at the downstream.

The temperature variations are sensitive to anode age. When the slots are not immersed yet, the temperatures are constant up to 240 hours. This can be explained by the bubbles movement which tends to go directly upwards bath free surface without impacting the pot sidewall. This observation validates the numerical results of the configuration (1), shown on Figure 10.

In the same way, temperature levels are low after 460 hours when the slots are consumed. The bubbles are released under the anode and dispersed around it; thus, the bath mixing is very low near the pot sidewall. This observation validates the numerical results of the configuration (3) shown on Figure 10.

After 240 hours, the temperatures increase depending on whether the thermocouples are situated on upstream or downstream side and on their positions along the pot length side as well. This increase occurs clearly during the second phase of the anode cycle when the anodes are immersed into the bath. This observation validates the numerical results of the configuration (2) shown on Figure 10. The bubbles released from the slots push the bath towards the pot sidewall where strong recirculation zones are generated close to the wall, which can explain the temperature increase.

The lower increase of temperatures at the upstream than downstream can be explained by the MHD driven flow behavior in the pot. From the velocity field streamlines seen in Figure 2, the eddies are counterclockwise from the downstream towards the upstream side. This trend seems to push the bubbles towards the sidewall in downstream side and slowdown them in upstream side. This can explain the higher increase of the temperatures in the central at the downstream side rather than the upstream side. In addition, the velocity maximum is located at the corners at upstream side.

The temperatures increase is summarized in the Table 1. Each value in the table corresponds to the difference between the mean value (estimated between 400 and 424 hours) and the mean value of the first 240 hours.

Table 1. Temperature variation after 240 hours (°C)

Bath free surface level	Tapping side	Central (Tapping and fume side)	Fume side
Upstream	41	24	34
Downstream	36	47	28

Furthermore, the various thickness of the ledge described by Langlois et al. [15] can also explain the temperatures increase differences between the central, tapping and fume side. There is more ledge protection, in blue color, at downstream corners and long upstream side, than at the middle of the downstream side and at upstream corners. The red color represents the metal/bath not solidified (Figure 14).

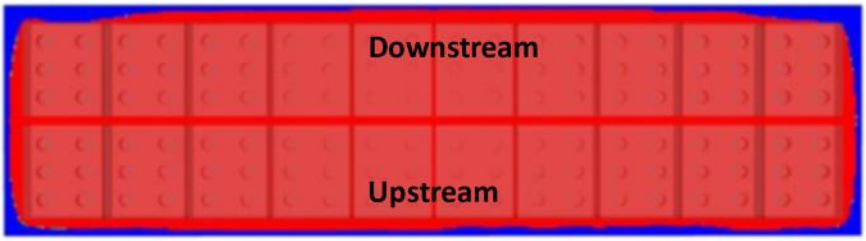

Figure 14. Ledge profile modeled on AP-40 from [15].

4. Conclusions and Future Work

In this work, Alucell latest development is presented. A model to consider the impact of CO_2 gas bubbles on the liquid flows in an aluminum reduction pot is developed. The modeling of the whole pot is enabled, thanks to the high calculation resources available at LRF.

The model highlighted that the bath flows are modified by the presence of the bubbles. The most important modifications of the velocity field take place in the channels (central and lateral). The gas volumetric flow rate is high mostly under the anodes. This gas distribution seems to be at the origin of the change on the metal pad interface, which tends to be higher under the anodes compared to a model without any gas.

Measurements of gas velocity as well as gas concentration are necessary to calibrate further the coefficients of the model, in particular the amplitude of the drag coefficient *D*. Moreover, the velocities are also dependent on the boundary conditions, through the friction coefficients that were used. With these measurements, the calibration of these coefficients will be performed.

The impact of inclined slots on the bath flows is noticeable in the lateral channels, leading to high mixing flow near the pot sidewall and it is responsible for the wall temperatures increase during the anode changing cycle.

Investigations should be done to study the impact of the modified velocity on alumina dissolution in the pot, using alumina dissolution model [16]. Furthermore, further R&D efforts will more precisely investigate the impact of the gas bubbles on the ledge profile, using the MHD-TE Alucell model [16].

However, when the whole pot is modeled with all anodes slotted, a large number of mesh elements is required, which makes the calculations impossible. Work is currently underway as part of a recent PhD. thesis in collaboration with EPFL, to develop a methodology to optimize and adapt the mesh in order to obtain more precise results. This ongoing work reduces the number of mesh elements, and the computational time of the calculations.

5. References

1. Alexandre L. Perron, Laszlo I. Kiss and Sandor Poncsák, Mathematical model to evaluate the ohmic resistance caused by the presence of a large number of bubbles in Hall-Héroult cells, *Journal of Applied Electrochemistry,* Vol.37, No. 3, 2007, 303-310.
2. Geoffrey Bearne, Derek Gadd, and Simon Lix, The impact of slots in reduction individual anode current variation, *Light Metals* 2007, 305-310.
3. W.E Haupin, A scanning reference electrode for voltage contours in aluminum smelting pots, *Journal of Minerals, Metals & Materials*, Vol.23, 1971, 46-49.
4. Laszlo Kiss et al., Simulation on the bubble layer in aluminum electrolysis pots, *Light Metals* 2005, 559-564.
5. Knut Bech et al., Coupled current distribution and convection simulator for electrolysis, *Light Metals* 2001, 463-468.
6. Y.F. Wang et al., Simulation of the fluid flow-related phenomena in the electrolyte of an aluminum electrolysis pot, *Metallurgical &Materials Transactions B*, Vol.42, 2011, 1051-1064.
7. S. Yang et al., Effects of slot cutting at prebaked anodes on bubble elimination in aluminum reduction pot, *Journal of Central South University*, Vol.43, 2012, 4617-4625.
8. X.W. Wang et al., Development and deployment of slotted anode technology at ALCOA, *Light Metals* 2007, 299-304.
9. Meijia Sun et al., Effect of slotted anode on gas bubble behaviors in aluminum reduction pot, *Metallurgical & materials transactions B*, Vol.48, 2017, 3161-3173.
10. Emile Soutter, *A mixture model to take into account diluted gas in liquid flow: applications to aluminum electrolysis*, PhD Thesis, Ecole Polytechnique Fédérale de Lausanne, Lausanne, Switzerland, 2021.
11. Steeve Renaudier et al., Alucell: a unique suite of models to optimize pot design and performance, *Light Metals* 2018, 541-549.
12. Michel Flueck et al., Scientific computing for aluminum production, *Int. J. Numer. Anal. Mod.*, Vol.6, Num.3, 2009, 489-504.
13. Michel Flueck et al., Numerical methods for ferromagnetic plates: applied and numerical partial differential equations, *Springer Netherlands*, 2010, 169-182.
14. Gilles Steiner, *Simulation numérique de phénomènes MHD: application à l'électrolyse de l'aluminium*, PhD Thesis, Ecole Polytechnique Fédérale de Lausanne, Lausanne, Switzerland, 2009.
15. Steve Langlois et al., 3D coupled MHD and thermo-electrical modeling applied to AP technology pots, *Light Metals* 2015, 771-775.
16. Thomas Hofer, *Numerical Simulation and optimization of the alumina distribution in an aluminum electrolysis pot*, PhD Thesis, Ecole Polytechnique Fédérale de Lausanne, Lausanne, Switzerland, 2009.